ISSN (Online) : 2319 - 8753
ISSN (Print) : 2347 - 6710

International Journal of Innovative Research in Science, Engineering and Technology

An ISO 3297: 2007 Certified Organization, Volume 2, Special Issue 1, December 2013

Proceedings of International Conference on Energy and Environment-2013 (ICEE 2013)

On 12th to 14th December Organized by

Department of Civil Engineering and Mechanical Engineering of Rajiv Gandhi Institute of Technology, Kottayam, Kerala, India

SHALLOW WATER BATHYMETRY USING LOG-LINEAR INVERSION TECHNIQUE: A CASE STUDY AT VIZHINJAM

Archa Raj, P. Sabu

Junior Engineer, Central Water Commission, Bangalore, 560013, India

Assistant Professor, Dept. of Civil, Engineering, CET Trivandrum, Kerala, 695016, India

ABSTRACT

Shallow water bathymetry of ocean is carried out to get the details of near shore bottom relief, which is important for navigation as well as for porting facilities. The conventional method of bathymetric derivation uses the echo sounder boarded on ship, for measuring water depth but they are labour-intensive and time-consuming. The remote sensing techniques derive water depth from multiple band satellite imagery, utilizing the optical properties of water column. The present work derives shallow water bathymetry using log-linear inversion technique from the multiple band Landsat Thematic Mapper image at a study area near Vizhinjam Harbour. The results obtained were validated using the sounding data taken using echo sounder which gave a RMSE of 1.9513 and the percentage error in analysis of depth using this method was obtained to be 26.22%.

NOMENCLATURE

ANN - Artificial Neural Networks
DN - Digital Number
NIR - Near Infra Red

MSS - Multispectral Scanner
TM - Thematic Mapper
L_{λ} - Radiance value in $Wm^{-2}\,sr^{-1}\mu m^{-1}$
L_{linear} - Linearized spectral value in $Wm^{-2}\,sr^{-1}\,\mu m^{-1}$
$L_{\max}$ - Maximum radiance value in $Wm^{-2}\,sr^{-1}\mu m^{-1}$
$L_{\min}$ - Minimum radiance value in $Wm^{-2}\,sr^{-1}\,\mu m^{-1}$

1. INTRODUCTION

Bathymetric information is of fundamental importance to coastal and marine planning and management, nautical navigation, and scientific studies of marine environments. Monitoring navigation channels for shipping traffic safety and mapping underwater sand bars, rocks, shoals, reefs and other hazardous marine features relies on up-to-date water depth measurement. Some nearshore activities like recreation, fishing, and aquaculture and offshore engineering works such as cable and pipeline laying, dredging, oil drilling, and beach nourishment, also require knowledge of bathymetry. For survey of bathymetry at synoptic scale, the remote sensing method may be a viable alternative to the conventional bathymetric mapping using echo sounders.

The fundamental physical principle underlying the retrieval of bathymetric information from optical remote sensing images is that when light passes through water it becomes attenuated by interaction with the water column. Deep areas appear dark on the image since the water absorbs much of the reflected light. Shallow areas appear lighter on the image since less light reflected from the seabed is absorbed in the passage through the water column.

There are many methods to derive bathymetry from satellite images. The simple radiative transfer model proposed by [1] uses a single band data to derive bathymetry from optical properties of water. The log-linear inversion model by [2] uses data from multiple bands. The non-linear bathymetric inversion model by [3] uses log-transformed band ratio to eliminate errors due to varying attenuation coefficients while considering more than one band. [4] derived shallow water bathymetry using Principal Component Analysis (PCA) based on bottom classification to extract the water depth information from multispectral data. [5] carried out a work on bathymetric depth derivation using artificial neural networks. ANN provides fast and practical solution for depth estimation in shallow waters, coupling temporal and spatial capabilities of remote sensing imagery with modelling flexibility of ANN. An indirect method of depth derivation was researched by [6]. In this method, the wavenumber and frequency of the waves were found out from satellite images and the depth of shallow waters was derived using the WSB method. [7] carried out a comparison of depths derived using the linear dispersion relation in an image and the lag correlation method using several images. [8] used the two-dimensional FFT to investigate the image spectrum and calculate the wave parameters from Synthetic Aperture Radar (SAR) images of ERS-1 satellite.

The basic premise of the log-linear inversion model is that attenuation varies spectrally. Upwelling radiance in spectral bands with high attenuation will be less than that of bands with lower attenuation. Therefore, increasing depth will induce faster decreases in radiance for spectral bands with stronger attenuation.

2. DATA

The Landsat 5 is a sun-synchronous satellite with near-polar orbit at an altitude of 705 km. Adjacent paths are covered with a separation of sixteen days. It carries two sensors namely the Multispectral Scanner (MSS) and the Thematic Mapper (TM). It has a swath width of 185 km. The research uses Landsat 5 TM image having seven spectral bands. The bands one to five and seven have a spatial resolution of 30m while the band 6 has a spatial resolution of 120m. The band 1 (0.45-0.52 µm), band 2 (0.52 - 0.60 µm) and band 5 (1.55 - 1.75 µm) images, after geometric correction, with ground control points and re-sampling, of the year 1990, 25th February was used in the present work.

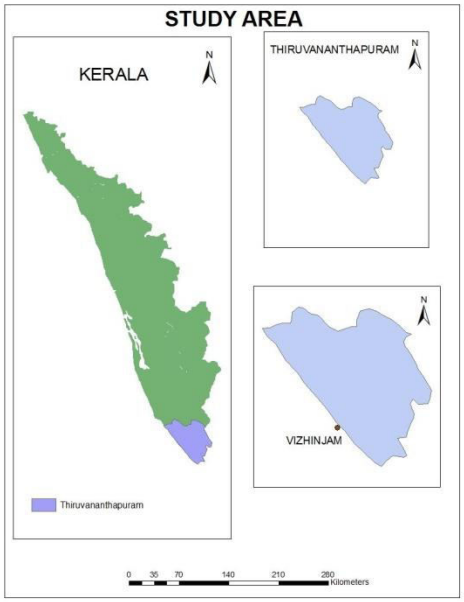

FIGURE 1 STUDY AREA

The image was freely downloadable from [14] and was downloaded band-by-band. They were then layer stacked together to view the image in true or false colour composites.

The study area chosen is the shallow water sea near to the Vizhinjam harbor region in the Arabian Sea. The reason for choosing this site was that the area has direct approach of waves without any obstruction in its path. Moreover, the in situ depth measurements are carried out regularly in this region. The study area was selected as a 2 km square area centered at 8^0 21' 34.25"E and 76^0 57' 14.35" N, towards the south of the Vizhinjam port.

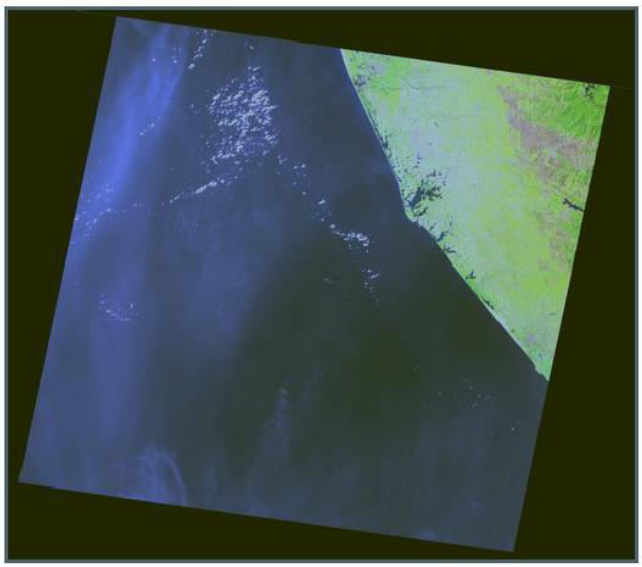

FIGURE 2 LANDSAT TM 5 IMAGERY

The actual in-situ depths of the location and the tidal data, which have been taken through soundings using echosounder, were obtained from the Hydrographic Survey Wing, Thiruvananthapuram. The

sounding data was used for training the dataset and also for the final validation of the results obtained using the Log Linear Inversion Technique. The location of Vizhinjam on Kerala map is shown in the figure 1 and imagery used for the work is shown in the figure 2.

3. METHODOLOGY

The water absorptivity varies spectrally from band to band. As the depth increases, the reflected irradiance decreases faster in the high-absorptivity spectral band (e.g. green band) than in the low-absorptivity band (e.g. blue band).

Assuming that the ratio of bottom reflectance between two spectral bands is constant for all bottom types within a given scene, [2] derived a log-linear inversion model for two or more spectral bands. The natural logarithm transformation produces a linear relationship between water depth and deep water-corrected radiances of spectral bands.

The total upwelling radiance recorded by the remote sensor is a sum of the bottom radiance, atmospheric path radiance and other losses. To decode water depth information, we need to disaggregate bottom radiance from total radiance. The various image processing steps adopted to extract the bottom radiance and finally the water depth from the available imagery data using loglinear inversion technique are shown in the flow chart given in figure 3.

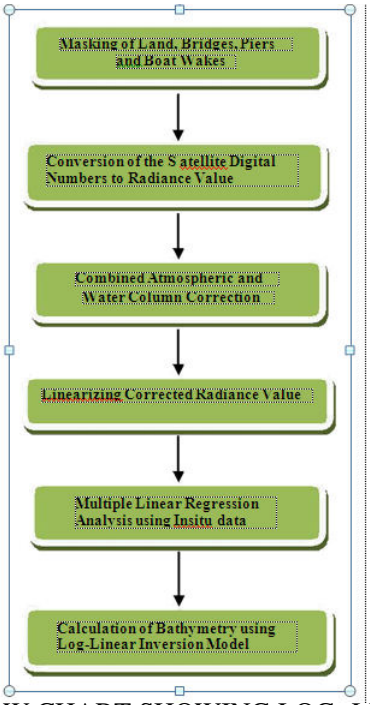

FIGURE 3 FLOW CHART SHOWING LOG- LINEAR INVERSION MODEL

The water region of the image was separated from the whole image using the Modified Normalized Differential Water Index. Here, the DN values of the green band and the SWIR band are considered.

$$MNDWI = \frac{Green - SWIR}{Green + SWIR} \qquad (1)$$

The value of MNDWI ranges from -1 to +1. The water regions have a value greater than zero while the non-water regions have a value less than or equal to zero.

The raw multi-spectral satellite data received from the satellite image is in the form of digital numbers (DN). This DN value was converted to radiance value using the following formula. [9]

$$L_\lambda = \left(\frac{L_{max} - L_{min}}{255} \right) DN + L_{min} \qquad (2)$$

where,

L_λ is the radiance value in $Wm^{-2}\, sr^{-1} \mu m^{-1}$, L_{max} represents the maximum radiance value in $Wm^{-2}\, sr^{-1} \mu m^{-1}$ and L_{min} represents the minimum radiance value in $Wm^{-2}\, sr^{-1} \mu m^{-1}$ and DN represents the digital number value.

The atmospheric and water column correction were carried out together by applying a modified deep water correction to the visible bands (blue and green bands) using the NIR band. [13]

$$L_i' = L_i - b_i (L_{NIR}) \qquad (3)$$

where, b_i is the regression line slope of band I (y axis) against the NIR band (x axis) . b_i is determined using a spatial subset of image pixels over optically deep water (>30 m) to obtain radiance values for the linear regression.

The corrected radiance values are then linearized using the following equation. [13]

$$L_{linear} = \ln (L_i' - L_{i\min}) \qquad (4)$$

where, L_{linear} is the linearized spectral value, L_i is the radiance value of band i after atmospheric and water column correction and $L_{i\,\min}$ is the minimum radiance of band i . The multiple linear regression analysis was carried out with depth as the dependant variable and the linearized spectral values of the bands considered as the independent variables.

$$D = a + b_i (x_i) + b_j (x_j) \qquad (5)$$

where, a = y-intercept, b = slope, x = linearized spectral value, i and j indicate spectral bands and D indicates the insitu depth values (sounding data). The variables x_i and x_j were drawn from the input image as it was processed.

The Log-Linear Inversion Model is given by

$$z = a_0 + \sum_{i=1}^{N} a_i \ln [L_i' - L_{i\,\min}] \qquad (6)$$

where, a_i (i = 0,1, . . . , N) are the constant coefficients, N is the number of spectral bands, L_i' is the remote sensing radiance after combined atmospheric and water column corrections for spectral band i , and is the deepwater radiance for spectral band i . The bands considered where blue and green. The y-intercept and the slope obtained from the multiple linear regression analysis were used here.

3. BATHYMETRIC DERIVATION

The bathymetric derivation using log-linear inversion techniques involved various image processing steps as mentioned in the methodology, where the initial DN number in the input image gets transformed to the depth value. The image processing was carried out using the software Erdas Imagine 2011.

3.1 Delineation of Water Surface and Masking of Land Area

Initially, the water surfaces were delineated using the Modified Normalized Differential Water Index (MNDWI). It was carried out using the equation 1. The fifth band (SWIR) and the second band (green) of the Landsat images were used for the calculation of modified NDWI. The water surfaces showed a value greater than one in the resultant image. It was assigned a black colour as shown in the figure 4. The boundaries of the water bodies were clearly visible indicating a demarkable variation from the non-water surfaces. Using this image, the water surfaces (assigned black in the modified NDWI image) of the band 1(blue) and the band 2 (green) were extracted separately. The non-water regions of the both these bands were masked.

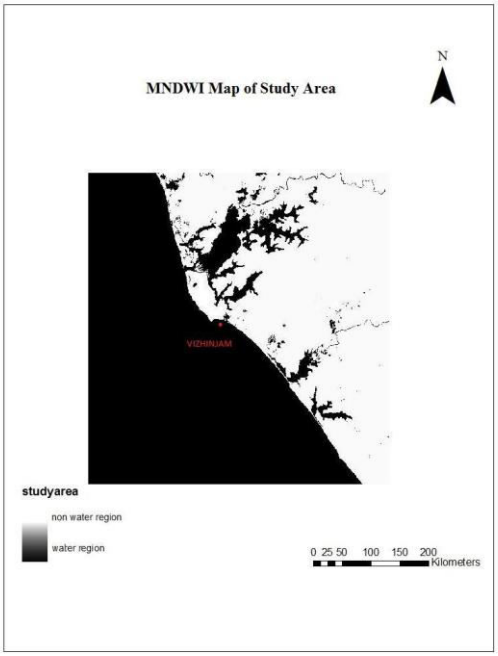

FIGURE 4 MODIFIED NDWI MAP OF STUDY AREA

3.2 Conversion of Satellite Digital Numbers to Radiance Value

The digital numbers were converted to radiance value using the equation 2. In the equation, the ^{L}max and the $L_{\min}$ values of Landsat TM image was taken from [10]. The radiance values were calculated separately for the blue, green and NIR bands.

3.3 Combined Atmospheric and Water Column Correction

The combined atmospheric and water column corrections were carried out using the equation 3. In the equation, the variable b_i is the slope of regression curve of band i along Y axis and NIR band along X axis. Linear regression was carried out between the radiance value of the NIR band and the blue and green band respectively. A subset of 32 x 32 pixels was selected over optically deep water in the NIR band as well as the blue and green bands to obtain radiance value for regression. The plot showing linear regression analysis between the radiance values of NIR band with blue and green bands is shown in the figure 5. The value of b_i obtained was 0.123 and 0.307 for blue and green bands respectively.

These values were used in equation 3 to deduce the radiance value after atmospheric and water column corrections.

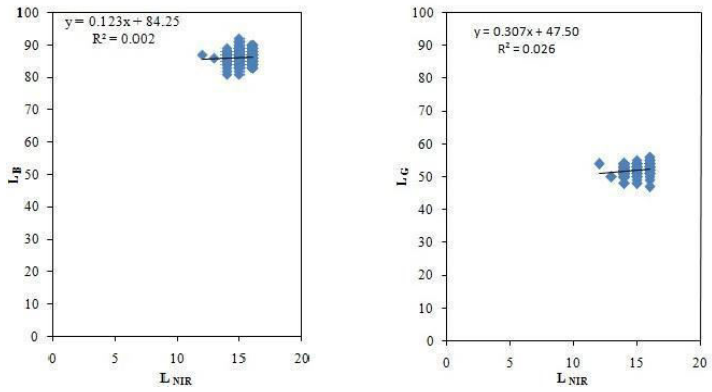

FIGURE 5 REGRESSION CURVE FOR DEEP WATER RADIANCE VALUES OF NIR BAND VS BLUE AND GREEN BANDS

3.4 Linearizing Corrected Radiance Value

After applying corrections, the spectral values were linearized using the equation 4. The variable $L_i^{'}$ is drawn from the input image as it is processed while $L_{i\ \min}$ is determined using a spatial subset over optically deepwater from the atmospheric and water column corrected image. A subset of 32 x 32 pixels was selected in the deep water region of the image after atmospheric and water column corrections for the blue and green bands and minimum radiance value within this subset was used in the equation 4.

3.5 Multiple linear regression analysis

The multiple linear regression analysis was conducted with insitu depth as the dependant variable and the linearized spectral values for the blue and green band as the independent variables using the equation 5.

Here, the independent variables were the linearized spectral values for blue and green bands. The outputs of interest were y-intercept, and the slope for each spectral band. Multiple linear regression analysis was carried out in Microsoft Excel 2007. The coefficient of regression obtained was 0.6772. The value of y-intercept and slopes (b_1 and b_2) obtained were 13.27, 0.386 and -0.610 respectively.

3.6 Derivation of Bathymetry using Log-Linear Inversion Technique

The y- intercept values and the slope values of the respective images obtained by multiple linear regression analysis was used in the equation 6 to get the derived depth for the study area. An average tide height of 0.8 m was deduced from the derived water depths to get the estimated water depth.

4. RESULTS

The shallow water depth of the study area was obtained using the log-linear inversion technique for the Landsat TM data. A plot of original sounding data (observed depth) along the Y-axis and the estimated depth along the X-axis was drawn as shown in figure 6. The RMSE and percentage error in estimation of shallow water bathymetry was also found out.

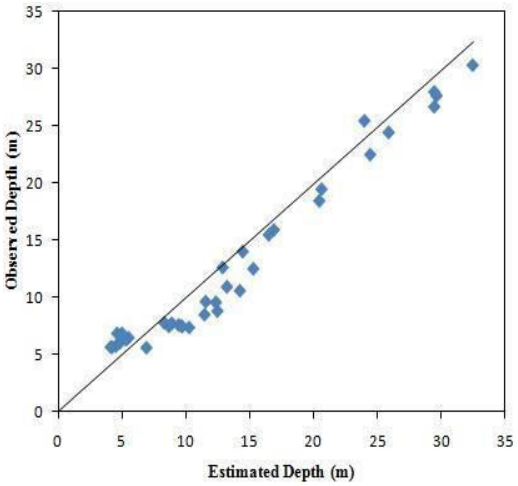

FIGURE 6 OBSERVED DEPTH VS ESTIMATED DEPTH

The RMSE obtained for the shallow water depth analysis using Landsat TM image was obtained to be 1.9513 and the percentage error in analysis of depth using this method was obtained to be 26.22%.

5. CONCLUSION

The log-linear inversion technique presented in this paper uses the blue, green and NIR band data of Landsat TM to derive the depth of shallow water sea at Vizhinjam, Thiruvananthapuram. The plot between the insitu data and the estimated depth was seen to give an RMSE of 1.9513. The percentage error in shallow water depth analysis using this method was obtained to be 26.22%. The plot between the insitu depth and the estimated depth gives a better result upto a depth of 12 meters, indicating that as the water becomes deeper, the accuracy of depth derivation from remote sensing techniques decreases. The accuracy level of analysis indicates that the method can be used to derive shallow water depths in areas where an idea of the bottom profile over large area is required in less time.

REFERENCES

[1] Lyzenga, D. R., 1978. "Passive remote sensing techniques for mapping water depth and bottom features". *Applied Optics*, 17 (3), pp. 379–383.
[2] Lyzenga, D. R., 1981. "Remote sensing of bottom reflectance and water attenuation parameters in shallow water using aircraft and Landsat data". *International Journal of Remote Sensing*, 1, pp. 71–82.
[3] Stumpf, K. Holderied, and Sinclair, M., 2003. "Determination of water depth with high-resolution satellite imagery over variable bottom types". *Limnology and Oceanography*, 48, pp. 547–556.
[4] Qing, D.W., Lei, P., Qin, Y., Hong, Z.Y., and Li, M.W., 2008. "PCA based on bottom classification applied in remote sensing bathymetry of shallow seawater".
[5] Ceyhun, O., and Yalcin, A., 2010. "Remote sensing of water depths in shallow waters via artificial neural networks". *Estuarine, Coastal and Shelf Science*, 89, pp. 89-96.
[6] Leua, L.G., Changb., H.W., 2005. "Remote sensing in detecting the water depths and bed load of shallow waters and their changes". *Ocean Engineering*, 32, pp.1174– 1198.
[7] Catalan, P., and Haller, M. C., 2006. "Nonlinear phase speeds and depth inversions".
[8] Dalrymple, R. R., Kennedy, A. B., and Kirby, J. T., 1998. "Determining depth from remotely-sensed images". *Coastal Engineering*, 76, pp. 2395-2408.
[9] Lillesand, T.M., Kiefer, R.W. and Chipman, J.W., 2004. "Remote Sensing and Image Interpretation". New York: JohnWiley and Sons.
[10] Chander, G., Markham, B. L., Helder, D. L., 2009. "Summary of current radiometric calibration coefficients for Landsat MSS, TM, ETM+, and EO-1 ALI sensors". *Remote Sensing of Environment*, 113, pp. 893–903.
[11] Lu, D., and Mausel, P., 2002. "Assesment of atmospheric correction methods for Landsat TM data". *International Journal of Remote sensing*, 23(13), pp. 2651-2671.
[12] Ji, L., Zhang, L., and Wylie, B., 2009. "Analysis of Dynamic Thresholds for the Normalized Difference Water Index". *Photogrammetric Engineering & Remote Sensing*, 75(11), pp. 1307–1317.
[13] Hogrefe, K. R., Wright, D. J., and Hochberg, E. J., 2008. "Derivation and Integration of Shallow-Water Bathymetry: Implications for Coastal Terrain Modeling and Subsequent Analyses". *Marine Geodesy*, 31, pp. 299–317.
[14] http://www.landsat.org.